BIBECHANA
Vol. 22, No. 1, April 2025, 1-14

ISSN 2091-0762 (Print), 2382-5340 (Online)
Journal homepage: http://nepjol.info/index.php/BIBECHANA
Publisher:Dept. of Phys., Mahendra Morang A. M. Campus (Tribhuvan University)Biratnagar

Computational evaluation on spectroscopic (FT-IR, Raman), electronic, biological, and NLO properties of cirsilineol by DFT, ADMET, and molecular docking method

Tirth Raj Paneru[1,4], Poonam Tandon[2], Bhawani Datt Joshi[3,*]

[1]*Department of General Science, Far Western University, Kanchanpur, Nepal*
[2]*Department of Physics, University of Lucknow, Lucknow-226007, India*
[3]*Department of Physics, Siddhanath Science Campus, Tribhuvan University, Mahendranagar, 10400, Nepal*
[4]*Central Department of Physics, Tribhuvan University, Kirtipur, Kathmandu, Nepal*
[*]Corresponding author. Email: bhawani.joshi@snsc.tu.edu.np

Abstract

Cirsilineol is a natural product that has pharmacological characteristics and is used to prevent the growth of cancer. This study aims to investigate the spectroscopic, electronic, and biological properties of drugs and predict their suitability for drug-like candidates to inhibit prostate cancer. The computational evaluation was performed with density functional theory (DFT) at B3LYP/6-311++G(d,p) level of theory and drug-like characteristics rendered from ADMET analysis. Spectral measurement for IR and Raman provided evidence of intramolecular hydrogen bonding of the OH group in ring R1. The electronic transition properties of the title compound were determined using TD-DFT with a polarized continuum model in solvent ethanol, resulting in a blue shift in absorption wavelength. The electrostatic potential mapped with the van der Wall surface predicted effective electrophiles and nucleophiles, allowing for the layout of intra- and intermolecular hydrogen bonds. The pharmacological properties of cirsilineol determined by ADMED analysis confirmed that it is non-toxic. To assess the biological performance of cirsilineol, molecular docking was performed with protein codes 1E3G and 1GS4, which showed inhibition action with binding affinity -7.7 and -7.8 kcal/mol, respectively.

Keywords

Cirsilineol, Vibrational spectra, Electrostatic potential, ADMET, van der Waals surface, UV-Vis spectra.

Article information

Manuscript received: September 25, 2024; Revised: December 7, 2024; Accepted: December 21, 2024
DOI https://doi.org/10.3126/bibechana.v22i1.70126

1 Introduction

Plant-derived products have pharmacological characteristics, so they have been used as medications for various types of diseases without harmful effects to the normal cells in body [1]. Flavonoids are pharmacologically significant phytochemical compounds found in fruits vegetables, and plant leaves [2]. The plant *Artemisia vestita* was used in traditional Chinese and Tibetan medicine for joint pain and inflammatory disease, which produces cirsilineol, also known as 4,5-dihydroxy-3,6,7-trimethoxyflavone and has antimicrobial, antioxidant, and anticancer properties [3, 4]. Research has demonstrated that it possesses anti-tumor properties and reduces the growth of human cancer cells [5]. Owing to its anticancer properties, it has been utilized for treating breast, prostate, and lung cancers, as well as other types of carcinomas, by enhancing the immune system [6, 7].

The literature reveals the curative and anticancer properties of cirsilineol using experimental and theoretical approaches [6,7]. Paneru *et al.* conducted a theoretical study on the conformational analysis, stability, reactivity, and drug potential of cirsilineol from DFT [8]. Literature indicates that Raman and IR spectra with vibrational analysis, non-linear optical properties as well as electron transition properties based on UV-Vis spectra analysis, have not been conducted yet. This study is primarily focused on the investigation of vibrational spectra, electronic transitions, and the more exact prediction of reactive sites in cirsilineol. For this study, quantum chemical calculations were performed on the title molecule using density functional theory and the B3LYP hybrid functional with basis set 6-11++G(d, p). This study uses potential energy distribution calculations to conduct a comprehensive spectroscopic investigation. The electrostatic potential was determined by the ESP surface analysis, which provides information about the reactive sites of the molecule. The nonlinear optical (NLO) properties of the title compound were also investigated in terms of dipole moment, polarizability, and hyperpolarizability to provide insight into its use as an NLO material. The natural charges on each atom were determined by natural population analysis (NPA). The drug-like properties and toxicity of the molecule were also evaluated by ADMET analysis. Finally, molecular docking was carried out to evaluate the anti-cancer effect of cirsilineol against protein codes of androgen receptor by detecting binding sites and binding affinity of the title molecule with the target protein codes.

2 Materials and Methods

2.1 Computational details

Geometry optimization of the molecule should require to commence the present work, which was accomplished by density functional theory in the Gaussian 09 software package [9, 10]. The computations were carried out with the hybrid functional B3LYP in the basis set 6-311++G(d,p), the correlation effect, as proposed by Lee, Yang, and Parr, and the exchange interactions, as presented by Becke, are both described by the B3LYP hybrid functional [11–13]. The electronic transition in orbitals was visualized using GaussView 05 [14] . The confirmation of IR and Raman frequencies, as well as the optimized structure of the molecule, was identified using Chemcraft software [15]. Through the use of harmonic approximation, the IR absorption and Raman intensity of the optimized structure were determined. Multiwfn 8 and VMD 1.9.4 software were used to map the electrostatic potential (ESP) with the molecular van der Wall surface [16, 17]. With the polarized continuum model (PCM), the UV-Vis absorption of cirsilineol demonstrating electronic transition on molecular orbital was rendered in gaseous and solvent phases, using the TD-DFT/B3LYP/6-311++G(d,p) level of theory [18, 19]. The density of state (DOS) spectrum was produced with the GaussSum 3.0 software, with a full width at half maximum (FWHM) of 0.3 eV [20]. The energy gap in the DOS spectrum was then compared with the energy gap between highest occupied molecular orbital (HOMO) and lowest unoccupied molecular orbital (LUMO). To evaluate the ADMET properties of cirsilineol, the Swiss ADME and PKCSM online web tool was used [21,22]. Auto Dock Tools (ADT) version 1.5.4 has carried out the molecular docking of the molecule [23]. Finally, the binding positions of the title molecule with the PDB codes of the androgen receptor were displayed using Discovery Studio Visualizer 4.5 [24].

3 Results and Discussion

3.1 Geometry optimization

The compound cirsilineol (CID 162464) was downloaded from the PubChem database, [25] and optimized using density functional theory with the B3LYP/6-311++G(d,p) level of theory. The ground state energy of cirsilineol was found to be -767078.745 kcal/mol, which is identical to the energy (-767080.126 kcal/mol) for the most stable conformer of cirsilineol as evaluated by Paneru *et al.* using the same level of theory [8]. The optimized structure of cirsilineol with a numbering scheme on the atoms is shown in Fig. 1. The optimized structure was used for further study of the

title compound.

3.2 Vibrational Assignment

The use of vibrational spectroscopy, such as Fourier-transform infrared (FT-IR) and Raman, can generate important insights into the interactions and structure of molecules. Cirsilineol consists of 41 atoms with (3N-6) 117 modes of vibration, all of those being IR and Raman active. The spectral wavenumbers for IR and Raman were calculated at the B3LYP/6-311++G(d,p) level of theory, but they were overestimated due to anharmonicity, so they were reduced using the wavenumber linear scaling (WLS) factor [26]. The vibrational wavenumber calculations and potential energy distribution assignment were performed in Gar2ped in accordance with Pulay's recommendations [27, 28]. The Raman intensity was not directly obtained from DFT calculations it can be obtained from the Raman scattering cross-section. Raman scattering cross-section is proportional to the amplitude and provided by the following relation [29].

$$\frac{\partial \sigma_j}{\partial \Omega} = \left(\frac{2^4\pi^4}{45}\right)\left(\frac{(\nu_0-\nu_j)^4}{1-\exp\left[\frac{hc\nu_j}{kT}\right]}\right)\left(\frac{h}{8\pi^2 c\nu_j}\right)S_j$$

where, h, c, and k as a universal constant. S_j and ν_j be the scattering activity and predicted wavenumber of j^{th} mode , and ν_0 be the wavenumber related to the excited state. Simulated spectra are produced by convoluting each predicted vibrational mode with the computed Raman and IR intensities using a Lorentzian line shape with a full width at half maximum (FWHM) of 8 cm^{-1} [30]. Table 1 displays both the unscaled and scaled wavenumbers for FT-IR and FT-Raman, as well as their PED distribution. The graph of IR absorbance plotted against the scaled wavenumber, adjusted using the WLS factor derived from DFT calculations, is presented in Fig. 2. The graph for the Raman spectra obtained by plotting the graph between Raman intensity and scaled wave number is shown in Fig. 3. Using the potential energy distribution in Table 1, and the IR and Raman spectra shown in Figures 2 and 3, we illustrated the vibrational modes associated with the functional groups, rings, and methyl groups of cirsilineol in the following sections.

3.2.1 O-H Vibrations

Cirsilineol has two OH groups on rings R1 and R3. This group may be reactive parts of molecules, allowing it to participate in intra- and intermolecular hydrogen bonds. The stretching vibration of the free O-H group in ring R3 is 3624 cm^{-1}, while the stretching vibration of the O-H group in ring R1 is 3064 cm^{-1}. The stretching vibration of free OH in a similar type of flavonoid, such as kaempferol, was computed to be 3626 cm^{-1}; in quercetin, 3640, 3598 cm^{-1}; in myricetin, computed to be 3546, 3608 cm^{-1}; and in catechol, computed to be 3647 cm^{-1} using B3LYP/6-31+G(d,p) level of theory. These are in agreement with our result [31]. The stretching vibration of the O-H group in ring R1 was found to be lower, confirming the presence of O4-H31...O5 intra-molecular hydrogen bonding. The O-H vibration of rings R1 and R3 showed a sharp peak in both IR and Raman spectra, whereas the vibration of O-H in ring R1 shifted to the lower frequency in IR and Raman spectra. The deformation of O-H groups occurred at 1415 and 1195 cm^{-1}.

3.2.2 O-CH_3 Vibrations

There are three methyl moieties in cirsilineol, and each one can vibrate in the different ways, including stretching, deforming, and rocking. The methyl group exhibits asymmetric stretching in the range of 2970-2950 cm^{-1} and symmetric stretching in the range of 2880-2860 cm^{-1}. Asymmetric deformations should fall within 1470-1430 cm^{-1}, while symmetric deformations should be within 1380-1370 cm^{-1} [32]. Asymmetric stretching of the methyl group was computed to be 3009, 3006, 3002, and 2941 cm^{-1}, whereas symmetric stretching was obtained at 2977, 2972, 2900, 2899, and 2886 cm^{-1}. The asymmetric deformations of the methyl group were calculated at 1489, 1486, 1480, 1470, 1465, and 1464 cm^{-1}, while the symmetric deformations were determined at 1459, 1458, and 1447 cm^{-1}. Methyl moieties were found to be rocking at 1203, 1195, 1188, 1156, and 1155 cm^{-1}. These observations have shown that the calculated wavenumbers for various vibrations falls within the range reported in the literature.

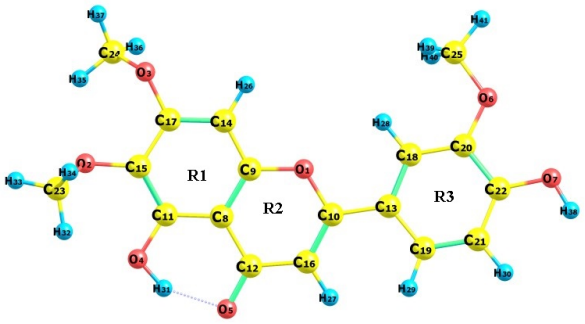

Figure 1: Optimized structure of cirsilineol showing intra-molecular hydrogen bonding (O-H...O) and numbering scheme on atoms.

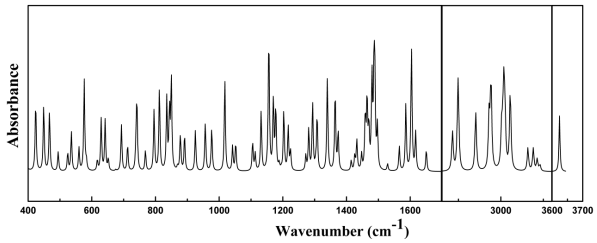

Figure 2: Calculated IR spectra of cirsilineol at the B3LYP/6-311++G(d,p) level of theory.

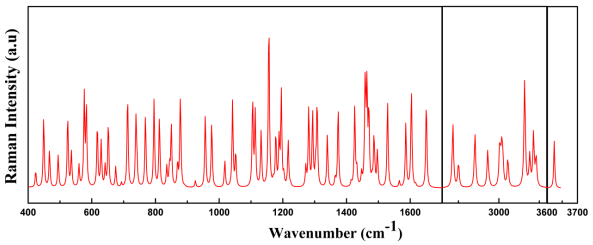

Figure 3: Calculated Raman spectra of cirsilineol at the B3LYP/6-311++G(d,p) level of theory.

3.2.3 Vibrations in ring R1

Ring R1 consists of one C-H moiety and three C-O moieties. The Stretching, in-plane

bending, and out-of-plane bending should all be in the range 3100-3000 cm^{-1}, 1350-950 cm^{-1}, and 1100-600 cm^{-1}, respectively [33]. Stretching of C-H was calculated to be 3076 cm^{-1}, with in-plane bending at 1170 cm^{-1} and out-of-plane bending at 835 cm^{-1}. C-C stretching in ring R1 occurred at 1651, 1617, 1566, 1697, 1632, 1364 and 1303 cm^{-1}. C-O stretching was obtained at 1224 cm^{-1} with a 22% PED contribution, whereas other C-O stretching had a lower PED contribution. Because the CH_3 group is attached to the C-O group, the in-plane and out-of-plane bending contributes significantly less in PED. The ring showed trigonal deformation at 712 cm^{-1} and asymmetric deformation at 576 cm^{-1}, with a lower contribution from PED. Additionally, the ring showed puckering and torsion at 768 and 629 cm^{-1}. Their contribution with the peak observed in IR and Raman spectra.

3.2.4 Vibrations in ring R2

Ring R2 contains one C-H moiety and one C=O group. The stretching vibration of C-H was obtained at 3076 cm^{-1} with in-plane deformations and out-of-plane deformations computed at 1281, 1272 cm^{-1}, and 850, 844 cm^{-1} respectively. The in-plane bending of C-H is a lower PED contribution. The stretching of CO occurred at 1605 and 1586 cm^{-1} with PED contributions of 21% and 15%, respectively; the lower PED contribution of the CO group is due to its participation in hydrogen bonding with the O-H group of ring R1. The stretching vibration of C=O aligns with those of myricetin at 1603 and 1570 cm^{-1}, as well as with quercetin at 1604 and 1571 cm^{-1} [31]. C-C stretching in ring R2 was calculated at 1586 and 1281 cm^{-1}. The asymmetric torsion, trigonal deformation, asymmetric deformation, and ring puckering occurred at 693, 524, 891, and 738 cm^{-1}, respectively, but had a lower PED contribution.

3.2.5 Vibration in Ring R3

In ring R3, there are three C-H groups with two C-O groups attached to hydrogen and methyl groups. The C-H stretching wavenumber were obtained at 3092, 3064, and 3022 cm^{-1}, while the in-plane bending was computed at 1529 and 1178 cm^{-1}, and the out of plane bending were occurred at 925 and 812 cm^{-1}. The stretching of C-O was computed at 1529, 1303, and 1272 cm^{-1}, while its in-plane bending and out-of-plane bending were computed at 560 and 467 cm^{-1}, respectively, with lower contribution in PED. The C-C stretching in the ring was determined at 1605, 1604, 1426, 1415, 1374, and 1293 cm^{-1}. The trigonal and asymmetric deformations in the ring occurred at 1272, 1052 cm^{-1} and 675, 642, 536, and 524 cm^{-1}, respectively. The puckering and asymmetric torsion values were calculated at 878, 741, 738, and 583 cm^{-1} and 812, 583, 467, and 449 cm^{-1}, respectively.

Table 1. Calculated wavenumbers of cirsilineol (in cm^{-1}) with their potential energy distribution.

Unscaled DFT	Scaled	**Potential Energy Distribution (PED)[a] (%)**
3830	3624	R3[ν(OH)](100)
3234	3092	R3[ν(CH)](99)
3227	3086	R2[ν(CH)](95)
3217	3076	R1[ν(CH)](99)
3203	3064	R3[ν(CH)](80)+R1[ν(OH)](13)
3202	3064	R1[ν(OH)](85)+R3[ν(CH)](13)
3157	3022	R3[ν(CH)](96)
3143	3009	ν_a(C24H$_3$)(100)
3140	3006	ν_a(C25H$_3$)(99)
3135	3002	ν_a(C23H$_3$)(99)
3107	2977	ν_s(C24H$_3$)(99)
3102	2972	ν_s(C23H$_3$)(98)
3067	2941	ν_a(C25H$_3$)(100)
3023	2900	ν_s(C23H$_3$)(96)
3021	2899	ν_s(C24H$_3$)(96)
3007	2886	ν_s(C25H$_3$)(100)
1682	1651	R1[ν(CC)(29)+δ_d(7)]+R2[ν(CC)(19)+ R2[ν(C=O)(10)+δ_d(6)]+δ(C11OH)(12)
1647	1617	R1[ν(CC)](26)+ R3[ν(CC)](19)+R2[ν(C=O)(11)+ν(CC)(8)]
1634	1605	R3[ν(CC)](36)+R2[ν(C=O)(21)+δ_{trig}(5)]
1633	1604	R3[ν(CC)](52)+R3[δ_{ip}(CH](12)+R3[δ_d](8)
1615	1586	R2[ν(CC)](24)+R2[ν(C=O)](15)+R3[ν(CC)](7)+R1[ν(CC)](6)+ν(C10C13)(6)
1593	1566	R1[ν(CC)](48)+R2[ν(CC)](15)+R1[δ_d](7)
1555	1529	R3[δ_{ip}(CH](35)+R3[ν(CC)](34)+R3[ν(C22O)](9)+R3[ν(C20O)](5)
1521	1497	R1[ν(CC)(29)+δ_{ip}(CH)(13)]+δ(C11OH)(15)+R2[ν(C=O)](8)+R1[ν(C17O)](8)
1513	1489	[δ_d(89)+ρ(9)](C24H$_3$)
1510	1486	δ_d(C23H$_3$)(89)+ρ(C23H$_3$)(9)
1504	1480	δ_d(C25H$_3$)(85)+ρ(C24H$_3$)(8)
1494	1470	δ_d(C25H$_3$)(92)
1488	1465	δ_d(C24H$_3$)(84)+ρ(C24H$_3$)(7)
1487	1464	δ_d(C23H$_3$)(82)+ρ(C23H$_3$)(7)
1482	1459	δ_s[(C25H$_3$)(53)+(C23H$_3$)(11)+(C24H$_3$)(9)]
1481	1458	δ_s[(C25H$_3$)(25)+(C23H$_3$)(25)+(C24H$_3$)(16)]
1470	1447	δ_s[(C24H$_3$)(31)+(C23H$_3$)(30)]+δ(C11OH)(13)
1454	1432	R1[ν(CC)](35)+δ_s[(C24H$_3$)(12)+ (C23H3)(7)]+R1[ν(C11O)](11)+R2[δ_d](7)
1447	1426	R3[ν(CC)](22)+R3[δ_{ip}(CH](8)+R2[ν(CC)](8)+δ_s(C25H$_3$)(6)+δ(C11OH)(6)
1436	1415	R3[ν(CC)](13)+δ(C11OH)(11)+R2[ν(CC)](9)+δ_s(C24H$_3$)(6)+R3[δ_{ip}(CH](5)
1393	1374	R3[ν(CC)](48)+δ(C22OH)(8)
1383	1364	R1[ν(CC)](31)+ R3[ν(CC)](13)+R1[ν(C11O)](7)+δ(C22OH)(6)
1358	1340	R1[ν(CC)](18)+R1[ν(C11O+ν(C17O)](16)+R3[δ_{ip}(CH](9)+R2[ν(C9O)](7)
1325	1308	R1[ν(CC)](24)+R3[δ_{ip}(CH](18)+R2[ν(CC)](6)+R1[ν(C17O)](6)
1320	1303	R1[ν(CC)](42)+R3[ν(CC)](15)+R3[ν(C22O)](9)+ν(C20O)](5)]+R3[δ_{ip}(CH](5)
1310	1293	R3[ν(CC)](24)+R3[δ_{ip}(CH](17)+R1[ν(CC)](23)+R3[ν(C22O)](6)
1298	1281	R2[ν(CC)](13)+R2[ν(C10O)](12)+R2[δ_{ip}(CH](10)+R1[ν(C15O)](8)
1288	1272	R3[δ_{trig}](19)+R3[ν(C20O)](12)+R2[δ_{ip}(CH](11)+R3[ν(C22O)](11)
1238	1224	R1[ν(C15O)](22)+R2[δ_{ip}(CH](14)+ρ(C23H$_3$)(14)+R1[δ_{trig}](6)+R1[ν(CC)](5)
1231	1217	ν(C10C13)(15)+R3[ν(C20O)](15)+ρ(C24H$_3$)(11)+R3[δ_{ip}(CH](8)

1217	1203	ρ(C24H3)(66)+R1[ν(C17O)](7)+ρ(C23H3)(5)
1208	1195	ρ(C24H3)(26)+R3[δin(CH](18)+δ(C22OH)(15)+ρ(C25H3)(9)+ρ(C23H3)(5)
1201	1188	ρ(C23H3)(44)+R1[δin(CH](8)+R1[δtrig](5)
1191	1178	R3[δin(CH](34)+ρ(C24H3)(15)+δ(C22OH)(14)+R3[ν(CC)](14)+ρ(C25H3)(5)
1183	1170	R1[δin(CH](30)+R2[ν(C9O)](13)+R1[ν(C17O)](9)+R1[ν(CC)](7)
1169	1156	ρ(C25H3)(69)+ρ(C24H3)(25)+δa(C25H3)(5)
1168	1156	ρ(C23H3)(92)
1167	1155	ρ(C24H3) (91)+δa(C24H3)(5)
1143	1132	δ(C22OH)(22)+R3[ν(CC)](20)+R3[δin(CH](18)+ν(C25O)(7)+R3[ν(C22O)](7)
1124	1113	R1[ν(C24O)](17)+R1[ν(C17O)](16)+R2[ν(CC)](10)+R1[δa](6)
1116	1105	R2[ν(C9O)](25)+R1[ν(C11O)](15)+R2[ν(C10O)](7)+R1[δtrig](6)
1061	1052	ν(C25O)(32)+R3[ν(CC)](19)+R3[δtrig](11)+R3[δin(CH](7)
1051	1042	ν(C25O)(30)+R2[ν(C10O)](12)+R1[ν(C23O)](11)+R3[δtrig](7)+R2[δin(CH](5)
1026	1018	R1[ν(C23O)](47)+R1[ν(C24O)](15)
984	977	R1[ν(C24O)](45)+R1[ν(C23O)](11)+R1[δa](5)+R2[δtrig](5)+R1[ν(C17O)](5)
963	956	R2[ν(C10O)](15)+R2[δtrig](11)+R1[ν(C23O)](6)+ν(C25O)(5)+R3[ν(C20O)](5)
931	925	R3[oop(CH)](85)+R3[puck](7)+R3[τa](5)
897	891	R2[δtrig](24)+R1[δin(C11O](11)+R1[ν(C15O)](7)+R1[δin(C15O](6)
883	878	R3[oop(CH)](65)+R3[puck](13)+R3[oop(CC)](5)+R3[oop(C20O)](5)
874	869	τ(O4C)(92)
854	850	R2[oop(CH)](53)+R2[oop(C=O](10)+R2[puck](7)+R3[δtrig](5)
848	844	R2[oop(CH)](23)+R3[δtrig](12)+R1[oop(CH)](11)+R2[oop(C=O](5)
840	835	R1[oop(CH)](60)+R1[puck](13)+R1[oop(C17O)](7)
816	812	R3[oop(CH)](62)+R3[oop(C22O)](12)+R3[τa](8)+R3[puck](5)
799	796	R3[ν(CC)](30)+R3[ν(C20O)+ ν(C22O)](20)+R3[δa](8)+δ(C20OC)(7)
771	768	R1[puck](38)+R1[oop(C11O)](20)+R1[oop(C15O)](17)+R1[oop(C17O)](9)
744	741	R3[puck](34)+R3[oop(C22O+C20O)](21)+R2[oop(C=O](12)+R1[τa](7)
741	738	R3[puck](22)+R2[puck](16)+R2[oop(C=O](13)+R3[oop(C22O)](10)
714	712	R1[δtrig](19)+R1[δa](10)+R2[δin(C=O](9)+R2[δin(CC)](7)+R1[ν(C15O)](7)
695	693	R2[oop(CC)](50)+R2[puck](13)+R2[τa](10)+R3[oop(C20O)](7)
677	675	R3[δa](16)+R1[δin(C17O](10)+R2[δa](9)+R2[δtrig](8)+R3[δtrig](5)
653	652	R1[oop(C11O+C17O)](34)+R1[τa](18)+R2[oop(C=O](12)+R1[puck](11)
643	642	R2[δa](17)+R3[δa](12)+R1[ν(CC)+ δa(5)](11)+R1[δin(C11O](7)+R2[ν(CC)](5)
630	629	R1[τa](26)+R1[puck](25)+R1[oop(C11O+C17O)](15)+R2[puck](9)+R2[τa](9)
618	617	R3[δa](12)+R2[δa](10)+R2[δin(CC](10)+ R1[ν(CC)](9)+R1[δa](6)
583	583	R3[puck](13)+R3[τa](15)+R3[oop(CC)](10)+R2[oop(CC)](5)
576	576	R2[δin(C=O](24)+R1[δa](9)+R3[puck](8)+R3[τa](5)
560	560	R3[δin(C22O+ C20O)](34)+δ(C20OC)(7)+R2[δin(C=O](6)+R3[δin(CC](5)
536	536	R3[δa](19)+R1[δa](11)+R1[oop(C11O)](9)+δ(C15OC)(8)+δ(C20OC)(6)
524	524	R2[δa](29)+R1[δa](14)+R3[δa](13)+δ(C20OC)(5)+δ(C15OC)(5)
494	494	R2[δa](25)+δ(C15OC)(13)+R1[oop(C11O+ C15O)](13)+R3[δa](9)
467	467	R3[oop(C20O+C22O)](44)+R3[τa](36)+R3[oop()](22)+R3[τa](10)
448	449	R1[oop(C15O+ C11O)](16)+R1[δa](13)+ δ(C20OC)(7)+δ[oop(C11C8C9)(6)
423	424	R1[δin(C11O](27)+R1[δa](11)+δ(C17OC)(7)+R1[τa](6)+R1[oop(C17O)](5)
387	388	δ(C20OC)(15)+R1[τa](9)+R2[δin(C=O](8)+δ(C17OC)(8)+R3[δin(CC](7)

[a]Recommended vibrational normal mode assignments and potential energy distribution (PED)

Types of vibration: ν, stretching; ω, wagging; ρ, rocking; τ, torsion; γ, twisting; δ, deformation (bending), scissoring; oop, out-of-plane bending; in plane bending

Potential energy distribution (contribution≥5%)

3.3 Density of states (DOS)

When an electron transitions from the valence band to the conduction band, it results in a definitive change in the density of states [34]. The density of state spectra produced in the GaussSum 3.0 software with a full width at half maximum (FWHM) of 0.3 eV. The DOS spectrum for cirsilineol in the gaseous and solvent phase ethanol is shown in Fig. 3. Bonding interaction is suggested by a positive value on the DOS spectrum, anti-bonding is indicated by a negative value, and no bonding is indicated by a zero value. The green lines in the spectrum represent the highest occupied molecular orbital (HOMO), while the red lines represent the lowest unoccupied molecular orbital (LUMO). Acceptor orbitals are represented by virtual orbitals, and donor orbitals are represented by occupied orbitals. The high intensity of DOS represent multiple state of occupation at that energy level [35]. It was found that the energy gap in the DOS spectrum and the HOMO-LUMO gap in cirsilineol were identical. Cirsilineol is more reactive in the ethanol solvent and stable in the gaseous medium because the energy gap in the solvent phase was found to be less than that of the gaseous phase.

3.4 UV-V is spectrum and electronic transition

UV-Vis spectroscopy is the most fundamental tool for analyzing the absorption properties of pharmacological molecules, allowing us to better comprehend intra- and intermolecular interactions [36]. In this study, the UV-Vis spectrum was plotted in gaseous and solvent phase ethanol using TD-DFT in the IEF-PCM model to analyze the electronic transition between HOMO and LUMO [37]. Table 2 presents the major electron transitions along with their corresponding excitation energies, absorption wavelengths, and oscillator strengths. Fig. 4 displays the UV-Vis absorption spectra of cirsilineol in gaseous medium and solvent (water, ethanol, and methanol). The transition from HOMO→LUMO is the first excited state has an absorption wavelength of 363.40 nm with excitation energy of 3.41 eV in a gaseous medium and an absorption wavelength of 359.80 nm with excitation energy of 3.44 eV in solvent ethanol. The absorption in solvents shifted to a shorter wavelength is a blue shift, because the polarity of solvent increases. The decreases in absorption wavelength in solvent ethanol are due to the transition from n→π^* [38]. Figure 5 depicts the significant transition between HOMO and LUMO of cirsilineol in gaseous and solvent ethanol. The solvent facilitates charge transfer more readily than a gaseous medium; hence, the band gap in a solvent decreases, which increases its reactivity.

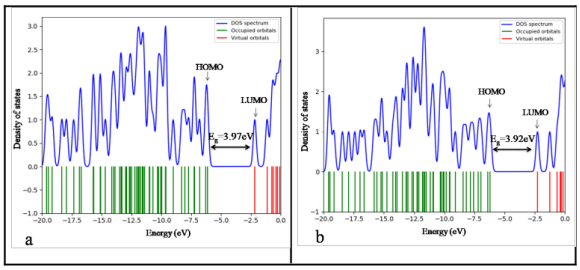

Figure 3a:Density of states spectrum of cirsilineol in (a) gaseous and (b) solvent (EtOH) phases.

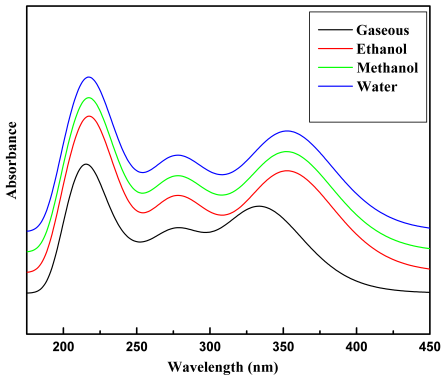

Figure 4: The UV-Vis absorption spectrum of cirsilineol (in gas and solvent phases).

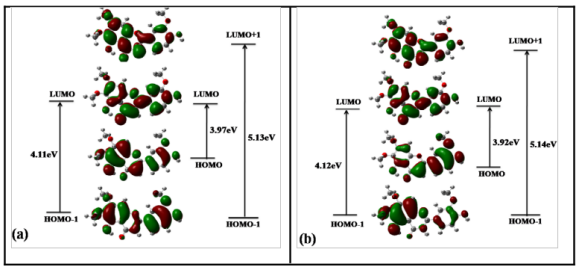

Figure 5: Major transition between HOMO and LUMO in gaseous and solvent EtOH phases.

Table. 2. The main contribution of electronic transition, with absorption wavelength, band gap, excitation energy, and oscillator strength in UV−Vis spectrum for cirsilineol in gaseous medium and in solvent.

Medium	Excited state	Excitation energy (eV)	λ_{max}	Oscillator strength (f)	Band gap (ev)	Major contribution (%)
Gaseous	1	3.41	363.40	0.0439	3.97	HOMO→LUMO (85%)
	2	3.70	334.79	0.4716	4.11	HOMO−1→LUMO (85%)
	7	4.66	265.70	0.0206	5.13	HOMO−1→LUMO+1(77%)
Ethanol	1	3.44	359.80	0.3378	3.92	HOMO→LUMO (74%)
	2	3.56	347.57	0.2746	4.12	HOMO−1→LUMO (75%)
	7	4.54	273.32	0.2421	5.14	HOMO−1→LUMO+1(80%)
Methanol	1	3.44	359.53	0.3309	3.92	HOMO→LUMO (73%)
	2	3.56	347.38	0.2729	4.12	HOMO−1→LUMO (74%)
	7	4.54	273.17	0.2456	5.14	HOMO−1→LUMO+1(81%)
Water	1	3.44	359.59	0.3440	3.92	HOMO→LUMO (74%)
	3	3.57	347.44	0.2604	4.13	HOMO−1→LUMO (75%)
	7	4.54	273.08	0.2477	5.14	HOMO−1→LUMO+1(80%)

3.5 Electrostatic potential (ESP) surface analysis

The foundation for the biological activity of a drug molecule can be laid by understanding the intermolecular interactions in molecules through the use of the electrostatic potential surface [39]. ESP displayed to the surface extrema of cirsilineol is shown in Fig. 6. The points of minimal and highest ESP were indicated in the figure by the blue and orange spots [40]. The regions of positive and negative potential on the molecule's surface were represented by the colors blue and red, respectively. The global minimum potential of the molecule was determined to be -38.38 kcal/mol, which is attributed to O5. The global maximum potential was found to be 56.88 kcal/mol, corresponding to H38. The largest positive potential on H38 is due to its attachment to oxygen, which attracts a large number of electrons from H38. This shows that the most effective electrophile and nucleophile for participating in intermolecular interactions are H38 and O5, respectively. The intermolecular hydrogen bonding formed by intermolecular interaction H38...O5 can form the crystal-packing of cirsilineol. All hydrogens in the molecule have positive potential, while oxygen has negative potential.

3.6 Natural population analysis

Mullikens charges are highly sensitive to the choice of basis sets; hence, natural population analysis is an alternative to it, which better describes the electron distribution in the compounds [41]. The natural population analysis determines the natural atomic orbitals and their occupancies and provides a natural atomic charge on each atom [42]. The natural charges on each atom of cirsilineol calculated at B3LYP/6-311++G(d,p) level of theory are presented in Table 3. The graph plotted between natural charges and each atom of the cirsilineol is also shown in Fig. 7. All the hydrogen atoms have positive charges, with H31 being the most electron-deficient and exhibiting the highest positive charge. Therefore, H31 is the most favorable site for nucleophilic attack. Conversely, all the oxygen atoms have negative charges, with O4 and O5 displaying the highest negative charges and possessing excess electrons. Consequently, O4 and O5 are potential sites for electrophilic attack. Due to this consequence the intra-molecular hydrogen bonding O4-H31...O5 was formed. C16, which has the highest negative charge of -0.3396 e, behaves as a nucleophile, while C12 exhibits the highest positive charge of 0.4840 e and acts as an electrophile.

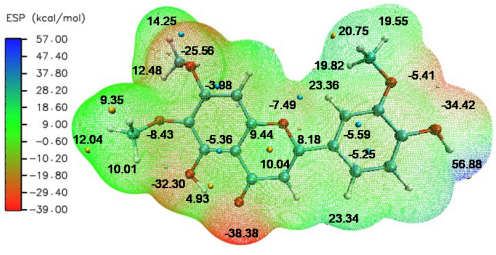

Figure 6: ESP mapped molecular vdW surface of cirsilineol.

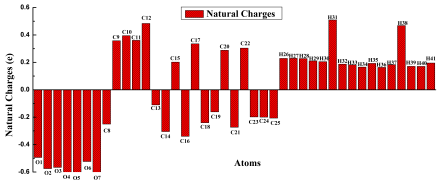

Figure 7: Distribution of natural charges calculated from natural population analysis.

Table 3. Natural charges calculated from natural population analysis on each atoms of cirsilineol.

Atoms	Natural Charge (e)	Atoms	Natural Charge (e)
O1	−0.4939	C21	−0.2734
O2	−0.5749	C22	0.3041
O3	−0.5662	C23	−0.1978
O4	−0.6787	C24	−0.1997
O5	−0.6503	C25	−0.2066
O6	−0.5234	H26	0.2292
O7	−0.6490	H27	0.2298
C8	−0.2501	H28	0.2277
C9	0.3580	H29	0.2105
C10	0.3949	H30	0.2052
C11	0.3607	H31	0.5093
C12	0.4840	H32	0.1872
C13	−0.1101	H33	0.1818
C14	−0.3047	H34	0.1656
C15	0.2020	H35	0.1926
C16	−0.3396	H36	0.1638
C17	0.3356	H37	0.1831
C18	−0.2404	H38	0.4686
C19	−0.1609	H39	0.1712
C20	0.2884	H40	0.1708
		H41	0.1953

3.7 Nonlinear optical (NLO) properties

When the electromagnetic field interact with the molecule it will causes formation of new field, change in phase, amplitude, frequency and other propagation properties of incident field which related with the nonlinear optical properties [43]. It gives key information in frequency shifting, optical communication, switching, data storage as well as signal processing [44]. The calculation of static dipole moment μ_0, mean polarizability $|\alpha_0|$, anisotropy of polarizability ($\Delta\alpha$), and first order hyperpolarizability β_0 of the most stable conformer of title molecule has been carried by using DFT at B3LYP/6-311++G(d,p) level of theory from the relations [45]:

$$\mu_0 = \left(\mu_x^2 + \mu_y^2 + \mu_z^2\right)^{\frac{1}{2}}$$

$$|\alpha_0| = \frac{1}{3}\left(\alpha_{xx} + \alpha_{yy} + \alpha_{zz}\right)$$

$$\Delta\alpha = 2^{-\frac{1}{2}}\left[\left(\alpha_{xx} - \alpha_{yy}\right)^2 + \left(\alpha_{yy} - \alpha_{zz}\right)^2 + \left(\alpha_{zz} - \alpha_{xx}\right)^2 + 6\alpha_{xx}^2\right]^{\frac{1}{2}}$$

$$\beta_0 = \left[\left(\beta_{xxx} + \beta_{xyy} + \beta_{xzz}\right)^2 + \left(\beta_{yyy} + \beta_{xxy} + \beta_{yzz}\right)^2 + \left(\beta_{zzz} + \beta_{xxz} + \beta_{yyz}\right)^2\right]^{\frac{1}{2}}$$

The components of static dipole moment, first order hyperpolarizability, mean polarizability and anisotropy of cirsilineol molecule are shown in Table 4. From the table it was found that cirsilineol have static dipole moment μ_0 was found to be 4.009 Debye, first order hyperpolarizability β_0 found to be (16.173×10^{-30} esu), and anisotropy of polarizability was found to be (107.698×10^{-24} esu). These values are larger than that of urea, hence it encourages the title molecule can be considered as an excellent NLO material [46].

3.8 ADMET properties analysis

Most pharmaceuticals in clinical trials fail to reach the market due to their limited potential and side effects, making the development of new medications difficult. ADMET analysis evaluates the absorption, distribution, metabolism, excretion, and toxicity of drug molecules [47]. The SwissAdme tool determined that cirsilineol has a molecular weight of 344.32, with four rotatable bonds, seven H-bond acceptors and 2 donors, 142.160 Å^2 topological polar surface areas (TPSA), and 91.44 molar refractivity. The bioavailability score and lipophilicity were found to be 0.55 and 2.53 respectively. All of these physicochemical parameters fall within the range of Lipinsky rules for drug likeness; hence cirsilineol can be used as an antimicrobial drug [48]. The solubility, TPSA, flexibility, molecular weight and lipophilicity except saturation of the title compound lie within the pink region of the radar plot given in Fig. 8 (a) indicating that cirsilineol is excellent in terms of bioavailability. The diagram of the boiled egg model in Fig. 8 (b) indicates that the red dots are located within the white region, suggesting that cirsilineol is effectively absorbed in the gastrointestinal tract and enhances bioavailability [49].

The pharmacokinetic properties determined by the online tool PKCSM as well as the ADMET properties for the title compound in terms of suitability for human administration are presented in Table 5. Cirsilineol has 100% intestinal absorption and a solubility of -3.326 mol/l, which is higher than

-4 mol/l. Additionally, it has a skin permeability of -2.75 cm/h, indicating desirable pharmacologic properties for absorption and distribution [50]. If the volume of distribution (VDs) is high, the drug will be distributed in plasma rather than tissue, which is in the desirable range for the title compound. BBB and CNS permeability were determined to be 0.738 (log BB) and -3.116 (log PS), respectively, indicating that they were unable to cross the blood-brain barrier and central nervous system. Additionally, it has a good metabolism and excretion, with a clearance of 0.638 (ml/min/kg). It is not positive to toxicity of AMES, indicating that it is mot mutagenic. The anticipated maximum dose for humans to be tolerated was 0.275 (mg/kg/day), which suggests a moderate level of tolerance. Finally, the fact that it responds negatively to enzyme inhibitory capacity, hepatotoxicity, and skin sensitivity suggests that it is not harmful. Hence, each of these qualities supported the medicinal nature of cirsilineol.

3.9 Molecular Docking

Molecular docking is a computational technique used to understand how drug molecules bind with the target receptor with the preferred orientation and find the binding affinity between them [51]. It has been reported that cirsilineol shows anticancer effects against human cancer cells, including prostate cancer. Literature has reported that androgen receptors have been associated with the progression of prostate cancer and are known to play a crucial role in male reproduction [52, 53]. cirsilineol inhibits the development of prostate cancer cells through the stimulation of ROS-mediated apoptosis [7]. In this study, we performed molecular docking with androgen receptor protein codes 1GS4 and 1E3G, which were downloaded from the protein data bank [54]. The water was taken out of the protein and Kollmann's charge was added in order to identify the active sites of the protein for a grid box of 60Åx60Åx60Å with a spacing of 0.375 Å. Figure 9 displays the binding modes illustrating the various interactions between cirsilineol and the protein codes 1E3G and 1GS4. For the protein codes 1E3G and 1GS4, the binding affinity and various docking evaluation parameters are shown in Table 6.

The active binding sites of protein codes 1E3G and 1GS4 both are confirmed at the centre having coordinates x = 6.786, y = 27.710 and z = 11.102. The binding affinity with 1E3G and 1GS4 were found to be -7.7 and -7.8 kcal/mol respectively. The inhibition constant for 1GS4 was found to be less as compared to 1E3G and RMSD between the initial structure and docked structure is 0.58 Å for 1GS4 hence title compound is a potential inhibitor of 1GS4.

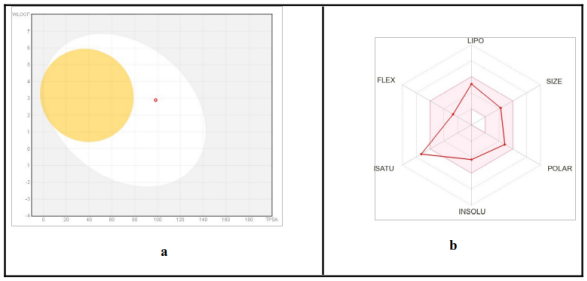

Figure 8: (a) Boiled-egg permeation plot and (b) Bioavailability radar plot of cirsilineol.

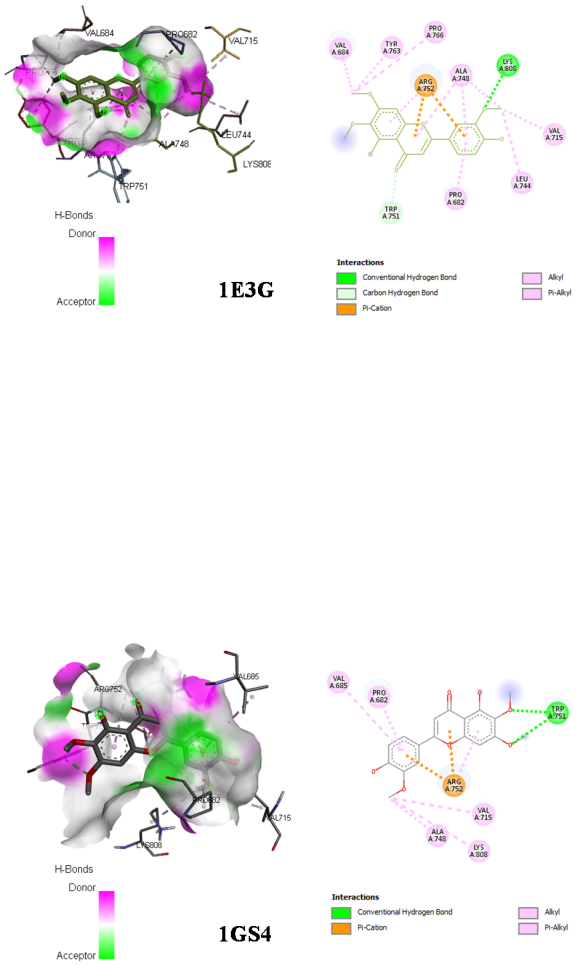

Figure 9: Docking of different protein codes of androgen receptor with cirsilineol showing best binding modes and interactions

Table 4. The dipole moment (μ_0), mean polarizability $|\alpha_0|$, anisotropy of polarizability ($\Delta\alpha$) and first hyperpolarizability (β_0) of cirsilineol calculated at B3LYP/6−311++G(d,p) level.

Dipole moment (Debye)		Polarizability (*10^{-24}esu)		Hyperpolarizability (*10^{-30}esu)	
μ_x	1.2563	α_{xx}	397.7424	β_{xxx}	-3107.77
μ_y	0.9179	α_{xy}	0.1747	β_{xxy}	-979.241
μ_z	0.2591	α_{yy}	275.2455	β_{xyy}	490.8527
μ_0	4.0095	α_{xz}	4.9012	β_{yyy}	-265.579
μ_0(Urea)	1.3732	α_{yz}	5.3397	β_{xxz}	-235.362
		α_{zz}	134.9457	β_{xyz}	82.2169
		$\|\alpha_0\|$	39.9911	β_{yyz}	-24.9539
		$\Delta\alpha$	107.698	β_{xzz}	-54.6484
		$\Delta\alpha$(Urea)	9.7710	β_{yzz}	36.771
				β_{zzz}	16.1729
				β_0	25.418
				β_0(Urea)	0.3728

Table. 5 ADMET properties of cirsilineol

Properties	Parameters	Predicted values	Units
Absorption	Water solubility	−3.326	Numeric (lo mol/L)
	Caco2 permeability	0.579	Numeric (log Papp in 10^{-6} cm/s)
	Intestinal absorption	100	Numeric (% Absorbed)
	Skin permeability	−2.75	Numeric (log Kp)
	P-glycoprotein substrate	yes	Categorical (Yes/No)
	P-glycoprotein I inhibitor	No	Categorical (Yes/No)
	P-glycoprotein II inhibitor	yes	Categorical (Yes/No)
Distribution	VDss (human)	−0.011	Numeric (log L/kg)
	Fraction unbound (human)	0.081	Numeric (Fu)
	BBB permeability	−0.738	Numeric (log BB)
	CNS permeability	−3.116	Numeric (log PS)
Metabolism	CYP3A4 substrate	No	Categorical (Yes/No)
	CYP1A2 inhibitor	Yes	Categorical (Yes/No)
	CYP2C19 inhibitor	Yes	Categorical (Yes/No)
	CYP2C9 inhibitor	No	Categorical (Yes/No)
	CYP2D6 inhibitor	No	Categorical (Yes/No)
	CYP3A4 inhibitor	Yes	Categorical (Yes/No)
Excretion	Total Clearance	0.638	Numeric (log ml/min/kg)
	Renal OCT2 substrate	No	Categorical (Yes/No)
Toxicity	AMES toxicity	No	Categorical (Yes/No)
	Max. tolerated dose (human)	0.275	Numeric (log mg/kg/day)
	hERG I inhibitor	No	Categorical (Yes/No)
	hERG II inhibitor	No	Categorical (Yes/No)
	Oral Rat Acute Toxicity (LD50)	2.263	Numeric (mol/kg)
	Oral rat Chronic toxicity (LOAEL)	1.933	Numeric (log mg/kg bw/day)
	Hepatotoxicity	No	Categorical (Yes/No)
	Skin sensitization	No	Categorical (Yes/No)
	T.*Pyriformis* toxicity	0.34	Numeric (log ug/L)
	Minnow toxicity	1.706	Numeric (log mM)

Table 6. Molecular docking parameters of cirsilineol with protein code (1E3G and 1GS4) of androgen receptor.

Selected PDB code and their resolution	Binding Affinity (kcal/mol)	H-Bond residues	Atoms	Bond length (Å)	Ligand efficiency	Inhibition constant (μM)	RMSD (Å)
1E3G (2.40 Å)	−7.7	LYS808	O6	2.38	0.30	2.24	1.67
1GS4 (1.95 Å)	−7.8	TRP751	O2	2.77	0.31	1.89	0.58
		TRP751	O3	2.48			

4 Conclusion

In this study, we employed DFT calculations to analyze the vibrational bands (FT-IR and Raman) associated with various moieties of cirsilineol. The FT-IR and Raman spectra were simulated, and the stretching vibrational wavenumber of the OH group in ring R1 was found to be lower due to the existence of intra-molecular hydrogen bonding O4-H31...O5. The DOS spectrum indicates an electron transition from the valence band to the conduction band, suggesting that the band gap in the ethanol solvent is 3.92 eV, while in the gaseous medium it is 3.97 eV. This suggests that the title compound is more reactive in an ethanol solvent. The transition of electrons between HOMO and LUMO is the first excited state for both gaseous and solvent mediums, with absorption wavelengths of 363.40 nm and 359.80 nm, respectively. The decrease in wavelength in the solvent indicates a blue shift, and there is a transition from n→*. The electrostatic potential mapped with the van der Waals surface showed that the global minimum and maximum potential of cirsilineol were determined to be -38.38 kcal/mol for O5 and 56.88 kcal/mol for H38, respectively. This implies that O5 and H38

are the effective nucleophile and electrophile, which could lay the groundwork for intermolecular hydrogen bonding in crystal packing. Natural population analysis predicted that O4 and H31 atoms had the highest negative and positive charge, respectively, supported the intra-molecular hydrogen bonding O4-H31...O5. The NLO study confirmed that cirsilineol can be used as an NLO material. ADMET analysis confirmed that the title compound is non-toxic and orally accepted. Finally, molecular docking with the androgen receptor shows that it has the lowest binding affinity of -7.8 kcal/mol with the protein code 1GS4 and the lowest inhibition constant, suggesting that cirsilineol may be an inhibitor of 1GS4.

Acknowledgments

T.R. Paneru acknowledges DST, India for granting a partial fellowship (INSA/DST-ISRF/2023/NEP/08/13), and B.D. Joshi acknowledges the University Grant Commission (UGC), Nepal for partial financial support to this work under the Faculty Research Grant (FRG-79/80-S&T-05).

Author Contributions

T.R. Paneru: Writing-original draft, investigation, and Formal analysis; P. Tandon: Software and supervision; B.D. Joshi: Writing-review, editing, and supervision.

Data Availability

The data supporting the findings of this study are available from the corresponding author upon reasonable request.

References

[1] D.K. Patel. Health benefits, therapeutic applications, and recent advances of cirsilineol in the medicine: Potential bioactive natural flavonoids of genus artemisia. *EMIDDT*, 23:894–907, 2023.

[2] A. Ullah, S. Munir, S.L. Badshah, N. Khan, L. Ghani, B.G. Poulson, A. H. Emwas, and M. Jaremko. Important flavonoids and their role as a therapeutic agent. *Molecules*, 25:5243, 2020.

[3] G.O. Kim, J.B. Heo, D.H. Park, G.Y. Song, and J. S. Bae. Antiplatelet aggregation properties of cirsilineol: A novel inhibitor of blood coagulation factor xa. *Pharmaceuticals*, 16:588, 2023.

[4] J. Wang, Y. Sun, Y. Li, and Q. Xu. Aqueous extract from aerial parts of artemisia vestita, a traditional tibetan medicine, reduces contact sensitivity in mice by down-regulating the activation, adhesion and metalloproteinase production of t lymphocytes. *Int. Immunopharmacol.*, 5:407–415, 2005.

[5] X. Sheng, Y. Sun, Y. Yin, T. Chen, and Q. Xu. Cirsilineol inhibits proliferation of cancer cells by inducing apoptosis via mitochondrial pathway. *J. Pharm. Pharmacol.*, 60:1523–1529, 2008.

[6] G. Pathak, S. Singh, P. Kumari, Y. Hussain, W. Raza, S. Luqman, and A. Meena. Cirsilineol inhibits proliferation of lung squamous cell carcinoma by inducing ros mediated apoptosis. *Food Chem. Toxicol.*, 143:111550, 2020.

[7] S. Wahab, A. Alsayari, A.B. Muhsinah, I. Ahmad, Md.S. Hussain, and J. Mallick. Cirsilineol inhibits the proliferation of human prostate cancer cells by inducing reactive oxygen species (ros) mediated apoptosis. *Evid. Based Complement. Altern. Med.*, 2022:1–7, 2022.

[8] T.R. Paneru, M.K. Chaudhary, P. Tandon, T. Chaudhary, and B.D. Joshi. Theoretical study on molecular stability, reactivity, and drug potential of cirsilineol from dft and molecular docking methods. *Chem. Phys. Impact*, 8:100641, 2024.

[9] P. Hohenberg and W. Kohn. Inhomogeneous electron gas. *Phys. Rev.*, 136:B864–B871, 1964.

[10] M.J. Frisch, G.W. Trucks, H.B. Schlegel, G.E. Scuseria, M.A. Robb, J.R. Cheeseman, G. Scalmani, V. Barone, B. Mennucci, G.A. Petersson, et al. *Gaussian 09, Revision A.02*. Gaussian Inc., Wallingford CT, 2009.

[11] C. Lee, W. Yang, and R.G. Parr. Development of the colle-salvetti correlation-energy formula into a functional of the electron density. *Phys. Rev. B*, 37:785–789, 1988.

[12] A.D. Becke. Density-functional thermochemistry. iii. the role of exact exchange. *J. Chem. Phys.*, 98:5648–5652, 1993.

[13] T.H. Dunning. Gaussian basis sets for use in correlated molecular calculations. i. the atoms boron through neon and hydrogen. *J. Chem. Phys.*, 90:1007–1023, 1989.

[14] A. Frisch, A.B. Nielson, and A.J. Holder. *GaussView user manual*. Gaussian Inc., Pittsburgh, PA, 2005.

[15] G. Zhurko and D. Zhurko. *Chemcraft graphical program for visualization of computed results*, 2015.

[16] T. Lu and F. Chen. Multiwfn: A multifunctional wavefunction analyzer. *J. Comput. Chem.*, 33:580–592, 2012.

[17] W. Humphrey, A. Dalke, and K. Schulten. Vmd: Visual molecular dynamics. *J. Mol. Graph.*, 14:33–38, 1996.

[18] R.E. Stratmann, G.E. Scuseria, and M.J. Frisch. An efficient implementation of time-dependent density-functional theory for the calculation of excitation energies of large molecules. *J. Chem. Phys.*, 109:8218–8224, 1998.

[19] M. Cossi, G. Scalmani, N. Rega, and V. Barone. New developments in the polarizable continuum model for quantum mechanical and classical calculations on molecules in solution. *J. Chem. Phys.*, 117:43–54, 2002.

[20] N.M. O'Boyle, A.L. Tenderholt, and K.M. Langner. cclib: A library for package-independent computational chemistry algorithms. *J. Comput. Chem.*, 29:839–845, 2008.

[21] A. Daina, O. Michielin, and V. Zoete. Swissadme: a free web tool to evaluate pharmacokinetics, drug-likeness and medicinal chemistry friendliness of small molecules. *Sci. Rep.*, 7:42717, 2017.

[22] D.E.V. Pires, T.L. Blundell, and D.B. Ascher. pkcsm: Predicting small-molecule pharmacokinetic and toxicity properties using graph-based signatures. *J. Med. Chem.*, 58:4066–4072, 2015.

[23] O. Trott and A.J. Olson. Autodock vina: Improving the speed and accuracy of docking with a new scoring function, efficient optimization, and multithreading. *J. Comput. Chem.*, 31:455–461, 2010.

[24] Accelrys Inc., San Diego. *Discovery Studio 4.5 Guide*, 2009.

[25] Pubchem compound summary for cid 162464, 2004.

[26] M.P. Andersson and P. Uvdal. New scale factors for harmonic vibrational frequencies using the b3lyp density functional method with the triple- basis set 6311+g(d,p). *J. Phys. Chem. A*, 109(14):2937–2941, 2005.

[27] J.M.L. Martin and C. Van Aslenoy. Gar2ped, a program to obtain potential energy distribution from gaussian archive record, 2007. University of Antwerp, Belgium.

[28] P. Pulay, G. Fogarasi, F. Pang, and J.E. Boggs. Systematic ab initio gradient calculation of molecular geometries, force constants, and dipole moment derivatives. *J. Am. Chem. Soc.*, 101(9):2550–2560, 1979.

[29] P.L. Polavarapu. Ab initio vibrational raman and raman optical activity spectra. *J. Phys. Chem.*, 94(18):8106–8112, 1990.

[30] B.D. Joshi, A. Srivastava, P. Tandon, and S. Jain. Molecular structure, vibrational spectra and homo, lumo analysis of yohimbine hydrochloride by density functional theory and ab initio hartree–fock calculations. *Spectrochim. Acta A Mol. and Biomol. Spectrosc.*, 82:270–278, 2011.

[31] G. Baranovic and S. Segota. Infrared spectroscopy of flavones and flavonols. reexamination of the hydroxyl and carbonyl vibrations in the relation to the interactions of flavonoids with membrane lipids. *Spectrochim. Acta A: Mol. Bimol. Spectrosc.*, 192:473–786, 2018.

[32] J. Coates. *Interpretation of Infrared Spectra, A Practical Approach.* Wiley, 1st edition, 2000.

[33] T. Chaudhary, M. Kumar Chaudhary, S. Jain, P. Tandon, and B. Datt Joshi. The experimental and theoretical spectroscopic elucidation of molecular structure, electronic properties, thermal analysis, biological evaluation, and molecular docking studies of isococculidine. *J. Mol. Liq.*, 391:123212, 2023.

[34] R. Rijal, M. Sah, H.P. Lamichhane, and H.S. Mallik. Quantum chemical calculations of nicotine and caffeine molecule in gas phase and solvent using dft methods. *Heliyon*, 8, 2022.

[35] C.S. Abraham, J.C. Prasana, S. Muthu, F. Rizwana B, and M. Raja. Quantum computational studies, spectroscopic (ft-ir, ft-raman and uv–vis) profiling, natural hybrid orbital and molecular docking analysis on 2,4 dibromoaniline. *J Mol Struct.*, 1160:393–405, 2018.

[36] M. Sirajuddin, S. Ali, and A. Badshah. Drug–dna interactions and their study by uv–visible, fluorescence spectroscopies and cyclic voltametry. *J. Photochem. and Photobio. B: Biology*, 124:1–19, 2013.

[37] J.B. Khadka and B.D. Joshi. Molecular electrostatic potential, homo-lumo and vibrational study of aristolochic acid ii using density functional theory. *BIBECHANA*, 12:40–52, 2014.

[38] A. Adeogun, N. Odozi, N.O. Obiegbedi, and O. Bello. Solvents effect on n→* and →* transition of 9-fluorenone. *African J. Biotechnol.*, 7:2736–2738, 2008.

[39] P.K. Weiner, R. Langridge, J.M. Blaney, R. Schaefer, and P.A. Kollman. Electrostatic potential molecular surfaces. *Proc. Natl. Acad. Sci. U.S.A.*, 79:3754–3758, 1982.

[40] T. R. Paneru, M. K. Chaudhary, P. Tandon, and B. D. Joshi. Cocrystal screening of benznidazole based on electronic transition, molecular reactivity, hydrogen bonding, and stability. *J. Mol. Mod.*, 2024.

[41] A.E. Reed, R.B. Weinstock, and F. Weinhold. Natural population analysis. *J. Chem. Phys.*, 83:735–746, 1985.

[42] S.A. Halim, A.B. El-Meligy, A.M. El-Nahas, and S.H. El-Demerdash. Dft study, and natural bond orbital (nbo) population analysis of 2-(2-hydroxyphenyl)-1-azaazulene tautomers and their mercapto analogues. *Sci. Rep.*, 14:219, 2024.

[43] B.D. Joshi. Nbo, chemical reactivity, thermodynamic properties and hyperpolarizability analysis of aristolochic acid ii. *BIBECHANA*, 14:86–97, 2016.

[44] C.E. Powell and M.G. Humphrey. Nonlinear optical properties of transition metal acetylides and their derivatives. *Coord. Chem. Revs.*, 248:725–756, 2004.

[45] J. Zyss. *Molecular nonlinear optics: Materials, physics, and devices*. Academic Press, 2013.

[46] C. Cassidy, J.M. Halbout, W. Donaldson, and C.L. Tang. Nonlinear optical properties of urea. *Optics Communications*, 29(3):243–246, 1979.

[47] L. Guan, H. Yang, Y. Cai, L. Sun, P. Di, W. Li, G. Liu, and Y. Tang. Admet-score - a comprehensive scoring function for evaluation of chemical drug-likeness. *Med. Chem. Comm.*, 10:148–157, 2019.

[48] C.A. Lipinski. Lead- and drug-like compounds: the rule-of-five revolution. *Drug Discovery Today: Technologies*, 1(4):337–341, 2004.

[49] S. Das, S. Nudrat, S. Maity, M. Jana, V.K. Belwal, and A. Singha Roy. Isoflavones and lysozyme interplay: Molecular insights into binding mechanisms and inhibitory efficacies of isoflavones against protein modification. *Chem. Phys. Impact*, 8:100643, 2024.

[50] A.H. Shamina, V. Ganesan, V.B. Jothy, A. Manikandan, S. Muthu, and S. Javed. Quantum chemical computations on molecular composition, spectroscopic properties, topology exploration, nlo, ligand protein interactions and pharmacokinetic evaluation of 8-hydroxyquinolium 3-nitrobenzoate. *Chem. Phys. Impact*, 8:100394, 2024.

[51] M.K. Chaudhary, T. Chaudhary, and B.D. Joshi. Simulated spectra (ir and raman), nlo, aim and molecular docking of carisoprodol from dft approach. *BIBECHANA*, 18(1):48–57, 2021.

[52] F. Alimirah, J. Chen, Z. Basrawala, H. Xin, and D. Choubey. Du-145 and pc-3 human prostate cancer cell lines express androgen receptor: Implications for the androgen receptor functions and regulation. *FEBS Letters*, 580(9):2294–2300, 2006.

[53] K. Fujita and N. Nonomura. Role of androgen receptor in prostate cancer: A review. *World J. Mens. Health*, 37(4):288–295, 2019.

[54] P.W. Rose, B. Beran, C. Bi, W.F. Bluhm, D. Dimitropoulos, D.S. Goodsell, A. Prlic, M. Quesada, G.B. Quinn, J.D. Westbrook, J. Young, B. Yukich, C. Zardecki, H.M. Berman, and P.E. Bourne. The rcsb protein data bank: redesigned web site and web services. *Nucleic Acids Research*, 39:D392–D401, 2011.